Duct Flow Nonuniformities – Effect of Struts in SSME HGM II$^+$ – Interim Report

25 January 1988

Contract NAS8-37359

Prepared for

NATIONAL AERONAUTICS AND SPACE ADMINISTRATION
MARSHALL SPACE FLIGHT CENTER, AL 35812

By

Roger Burke

Lockheed
Missiles & Space Company, Inc.
Huntsville Engineering Center
4800 Bradford Blvd., Huntsville, AL 35807

FOREWORD

This report documents interim numerical results obtained by personnel of the Computational Mechanics Section at Lockheed's Huntsville Engineering Center under Contract NAS8-37359, "Duct Flow Nonuniformities Study."

The NASA-MSFC Contracting Officer's Representative for this study is Dr. Paul K. McConnaughey, ED32.

ii

CONTENTS

LIST OF FIGURES

LOCKHEED-HUNTSVILLE ENGINEERING CENTER

CONTENTS (Concluded)

LOCKHEED-HUNTSVILLE ENGINEERING CENTER

ORIGINAL PAGE IS
OF POOR QUALITY

1. INTRODUCTION

This study consists of an analysis of flow through the Space Shuttle Main
Engine (SSME) Hot Gas Manifold (HGM) for the purpose of understanding and
quantifying the flow environment and, in particular, the flow through a region
of structural supports located between the inner and outer walls of the HGM.
The primary task of the study, as defined by NASA-MSFC, is to assess and
develop the computational capability of analyzing detailed three-dimensional
flow through the HGM support strut region to be incorporated into a full fuel-
side HGM analysis. Secondarily, computed results are to be compared with
available experimental results.

Figure 1 shows the SSME powerhead configuration. The turbine is run by a
hot gas, produced in the preburner by burning the fuel at high pressure and
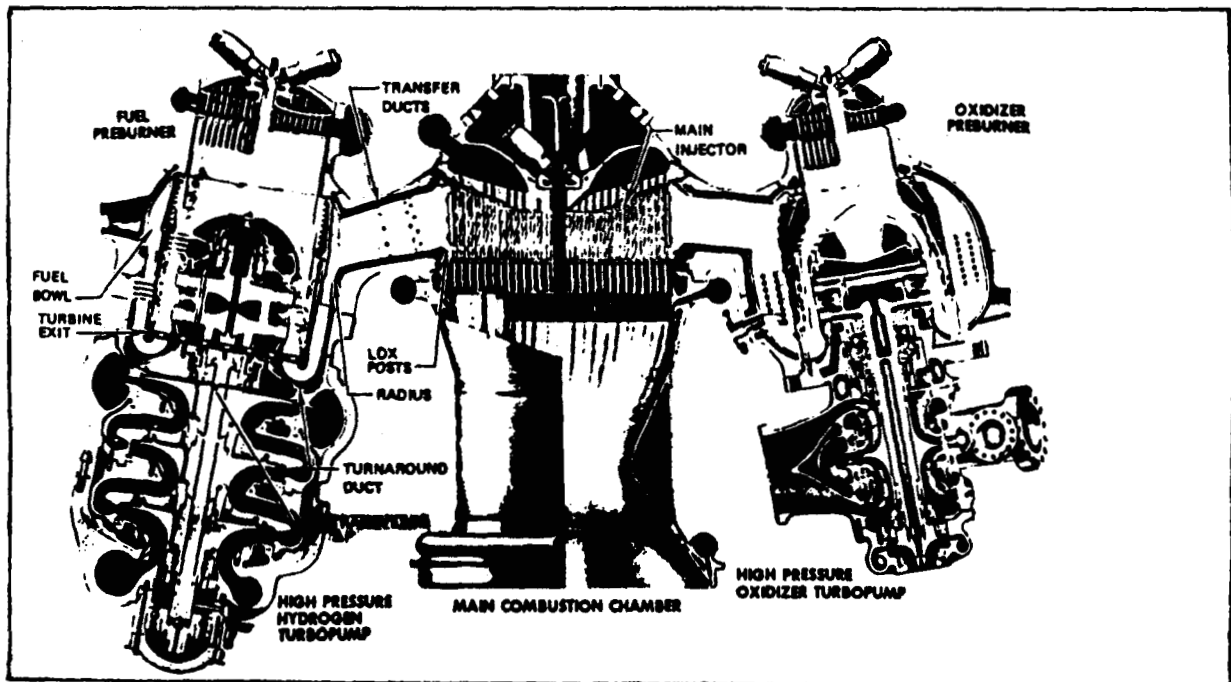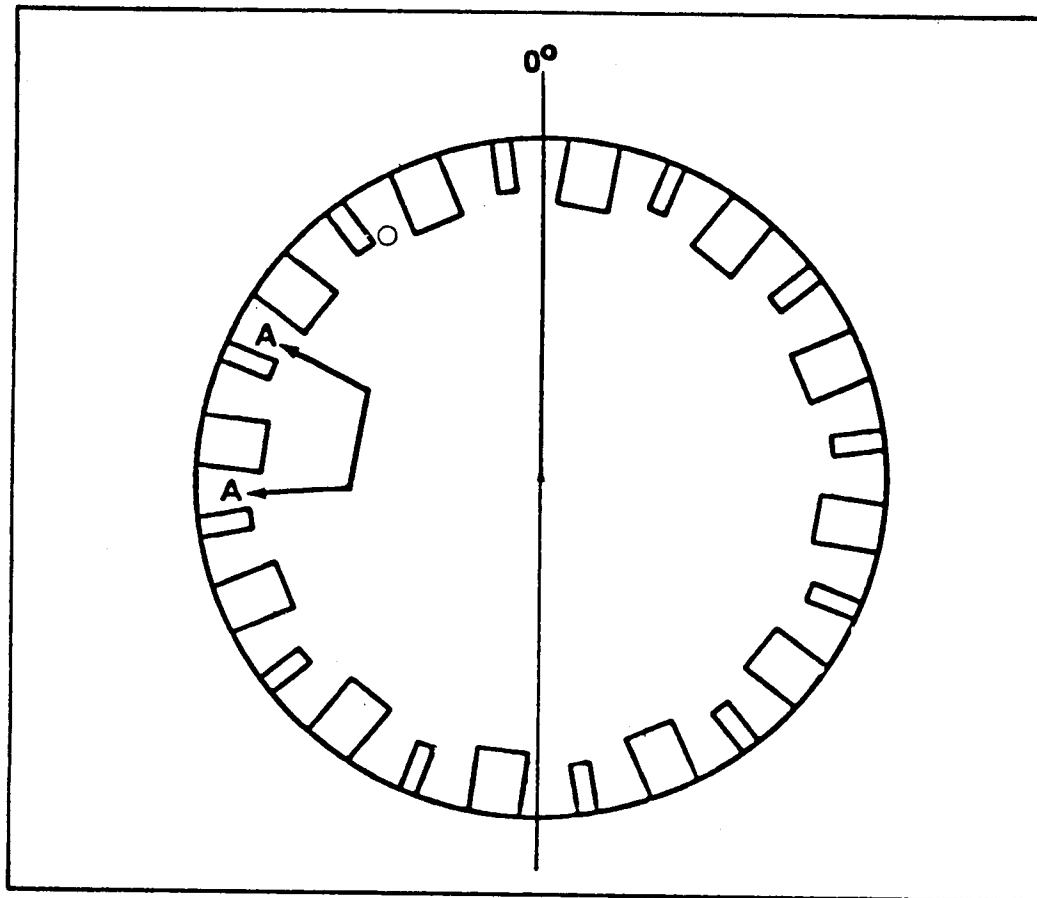high temperature. Having performed work on the turbine, this gas enters an

Fig. 1 SSME Powerhead Configuration

1

annular turnaround duct (TAD), which changes the direction of the mean flow by 180 deg. The gas then passes through an assembly of struts and posts before diffusing into a fuel bowl. The gas flows from the fuel bowl into the main injector through several transfer ducts. The high gas temperature causes the flow to be practically incompressible, with a Mach number of less than 0.12.

A more detailed picture of the strut-post assembly is seen in Fig. 2a, which presents an idealized cross-sectional view of the TAD, with the flow direction normal to the plane of the paper. Figure 2b shows a different perspective, with the flow direction in the plane of the paper.

As a first step toward simulating the three-dimensional viscous, turbulent flow in the HGM strut region, two simplified test geometries were investigated, and will be the major focus of this interim report. These geometries consist of two-dimensional flow around a strut, and three-dimensional flow around a strut in an annulus. Both laminar and turbulent calculations were performed. A multi-zone procedure was implemented to calculate two-dimensional laminar flow over two struts placed in parallel, with each strut confined to a separate computational zone. Details of the approach used to numerically simulate these flow fields are contained in Section 2. Computational results are presented and discussed in Section 3, and concluding remarks are outlined in Section 4.

a.   Idealized Top View of TAD Strut and Post Assembly
     (Flow direction is normal to plane of paper.)

b.   View A, with Flow Direction in Plane of Paper

Fig. 2   Strut and Post Assembly

3

2. APPROACH

2.1 GENERAL DESCRIPTION

Computations were performed using the INS3D code for incompressible three-dimensional flow which was developed by Kwak et al. (Ref. 1). The code solves the full three-dimensional incompressible Navier-Stokes equations, using a pseudo-compressibility approach to handle the pressure. Reference 1 provides a detailed description of the INS3D methodology.

2.2 MULTIPLE-ZONE METHOD

The calculations in this study were performed on the NASA-Ames Cray X-MP 4/8, which has a maximum allowable CPU memory of approximately four million words. A full three-dimensional, viscous simulation of the flow in the HGM strut region will require more computational mesh points than can be handled by this size of storage, thus necessitating the use of a multiple-zone method. In this method, the solution is obtained by dividing the computational domain of interest into several zones, generating the grid for each zone separately, then solving the equations of motion in each zone to update the interior points. The points at the interface between zones are updated using a zonal boundary treatment which ensures smooth continuation of the solution between zones. Various zonal boundary strategies have been proposed (Ref. 2 and 3). The approach used in this study consists of a simple double-plane overlapping, as described by Chang et al. (Ref. 4) and Holst et al. (Ref. 5).

As an illustration of the zonal boundary treatment scheme, Fig. 3 shows a double-plane overlapping of two zones; the grid points of zone 1 are designated by circles, while those of zone 2 are marked by diamonds. The last two grid lines of zone 1 (j-1 and j) are seen to overlap with the first two lines
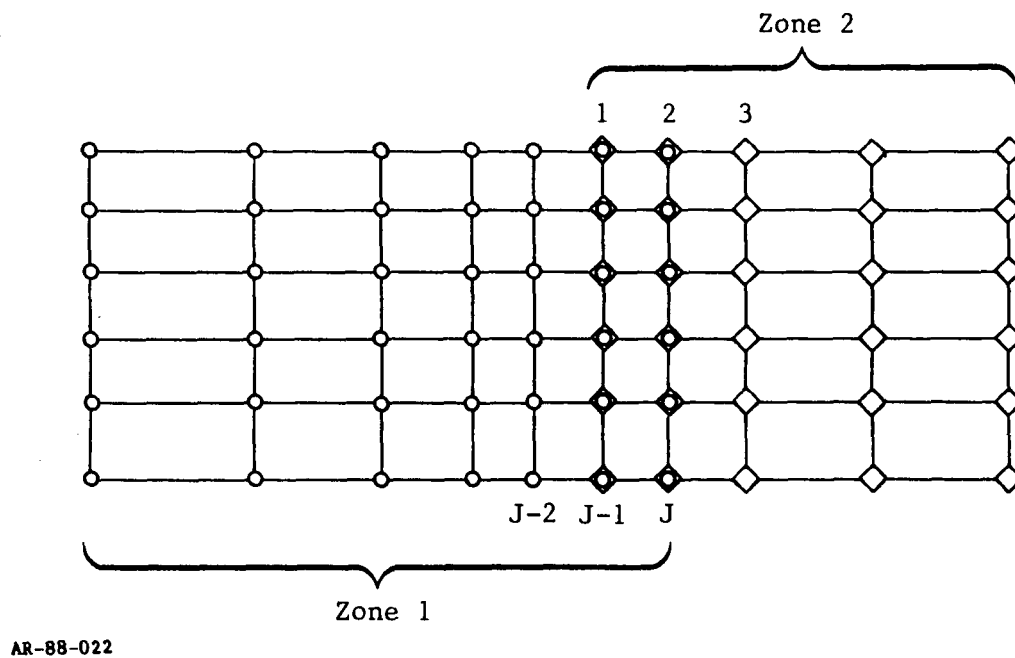
4

Fig. 3 Zonal Boundary Treatment Scheme

AR-88-022
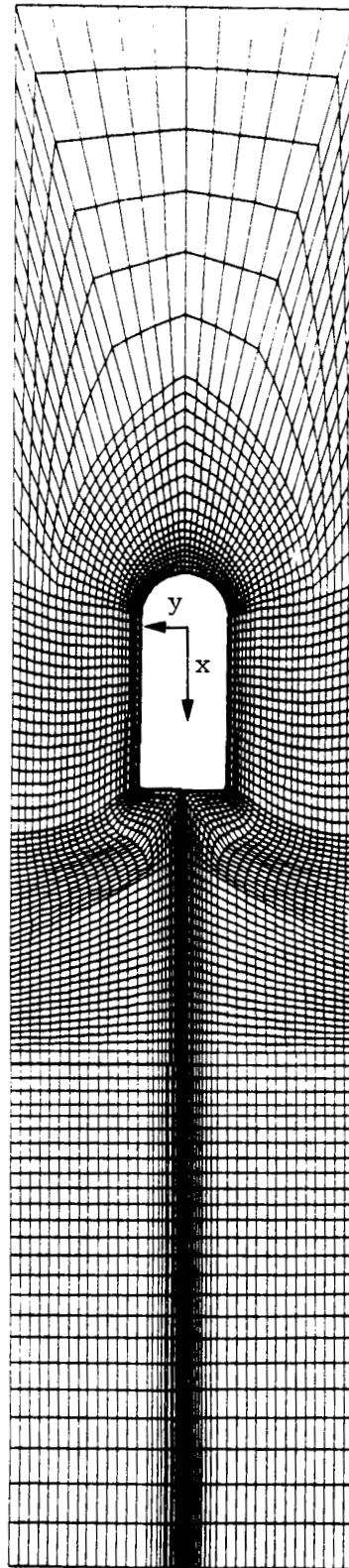
LOCKHEED-HUNTSVILLE ENGINEERING CENTER

Fig. 4 Mesh System Around Two-Dimensional Strut

6

of zone 2. Upon updating the interior nodes of zone 1 using the INS3D inte-
gration scheme, the values of the variables at the first line of zone 2 are
set equal to the updated values of line j-1 in zone 1. Next, the interior
points of zone 2 are computed, and the newly calculated values on line 2 in
zone 2 are used to update line J in zone 1. This procedure assumes that a
one-to-one correspondence exists between the nodes in each zone, which will be
the case for the calculations discussed here. In situations where a coarse
grid overlaps with a finer grid, an interpolation process is required to carry
the information from one grid to another (Refs. 4 and 5). Such an inter-
polation routine will be necessary to multi-block the computational zones
containing the struts with the relatively lower density grid of the TAD.

2.3 GRID

The test geometry grids used in the calculations presented here were
generated using the Lockheed algebraic grid generation code. The test geometry
strut has a 3:1 length-to-width ratio. The distance between struts is four
strut widths. The turnaround duct (TAD) is modeled as an annulus with an inner
radius of 6.5 and an outer radius of 8.5 strut widths. These dimensions do not
coincide with those of the strut assembly in the HGM; the actual dimensions
will be incorporated into the final computations.

Figure 4 shows the C-type mesh system around the two-dimensional strut.
The x-y Cartesian coordinate system is oriented so that x is in the streamwise
direction. There are 201 grid lines wrapped around the strut with 26 grid
lines extending away from the strut. The two-zone grid used in the multi-zone
calculations is presented in Fig. 5. The two zones are seen to overlap one
another by a double line of nodes. Computations are first performed on grid 1,
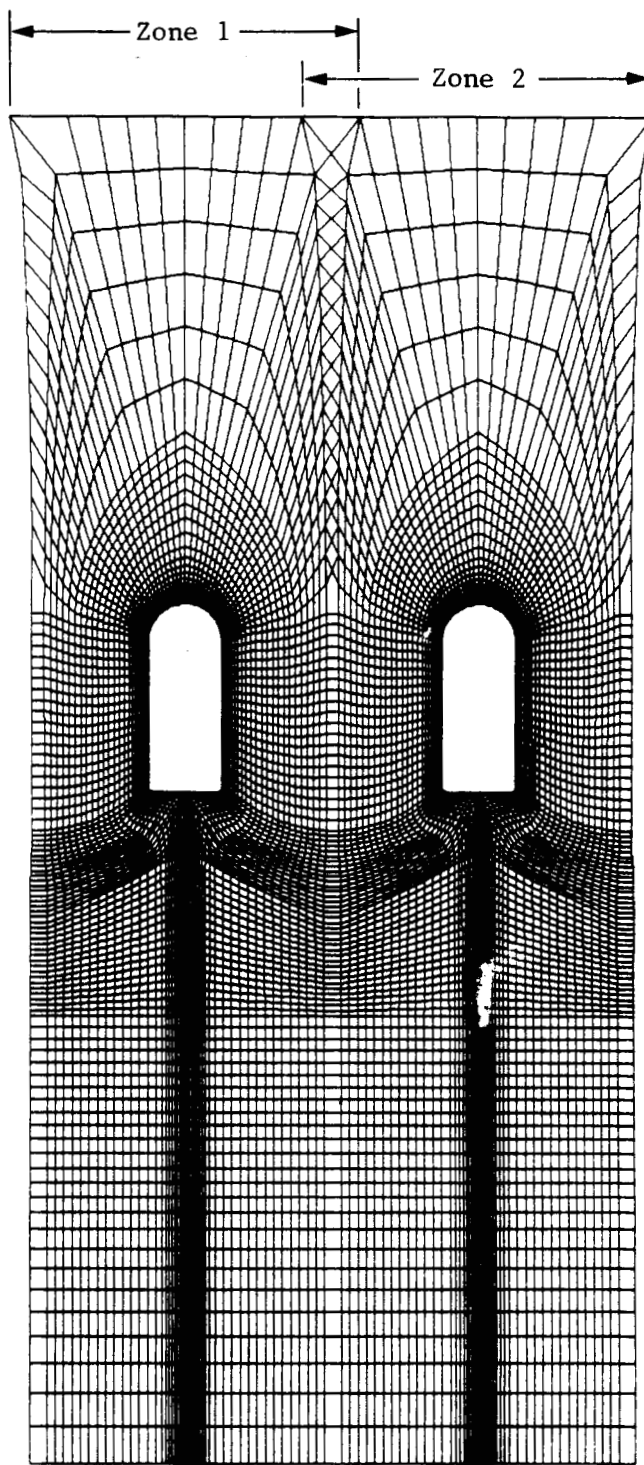and then on grid 2, with the zonal interface being treated as discussed
in Section 2.2.

7

Fig. 5 Two-Zone Grid Used in Multi-Zone Calculations

8

LOCKHEED–HUNTSVILLE ENGINEERING CENTER

The grid modeling a three-dimensional strut in an annulus contains 31 planes in the vertical (z) direction. In each annular plane the grid has the same configuration as the two-dimensional grid, resulting in a total of 162006 grid points for the three-dimensional geometry. Figure 6 shows that portion of the grid in the vicinity of the strut indicating all no-slip surfaces in the geometry.

For both the two-dimensional and three-dimensional grid the inlet plane is located a distance of 12 strut widths ahead of the strut. The exit plane is 18 strut widths downstream of the strut trailing edge.

2.4 BOUNDARY CONDITIONS

Explicit boundary conditions are used in the calculations. No-slip conditions are applied on the strut and annulus surfaces. The pressure on these surfaces is determined by requiring that the normal pressure gradient be zero, i.e.,

$$\frac{\partial p}{\partial \hat{\eta}} = 0 \tag{1}$$

where $\hat{n}$ represents the direction normal to a wall.

Conditions for the downstream boundary are the most difficult to provide, and they require careful specification to avoid numerical instabilities and nonconvergence. The downstream values of pressure and velocity are updated in the manner prescribed by Chang et al. (Ref. 4). In this approach, a second-order upwind extrapolation is first used to update the velocities normal to the exit plane. Next, these updated velocities are mass-weighted to conserve the inlet mass flux. A new pressure corresponding to these mass-weighted velocities is then determined to ensure conservation of momentum flux at the outflow.
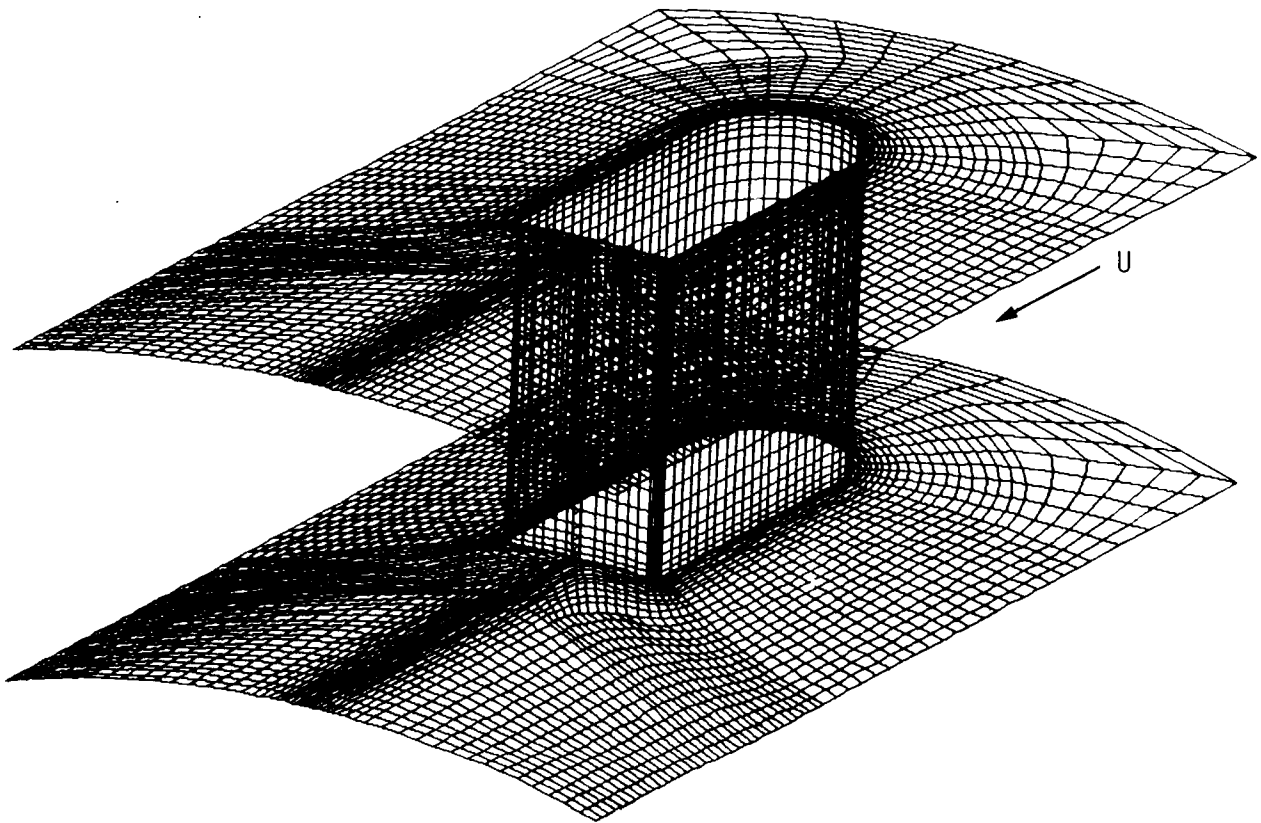
Fig. 6   Strut with Upper and Lower Annulus Surfaces

10

Periodic boundary conditions are applied at the lateral boundaries to simulate the effect of a row of struts, such as exists in the HGM. The posts, which are located midway between successive struts (Fig. 2b) are treated as no-slip boundary nodes. To date, the posts have been included in two-dimensional laminar calculations only. For the two-dimensional computations uniform static pressure and velocity is assumed known and held fixed at the inlet. For the three-dimensional calculation of a strut in an annulus, a uniform static pressure is held fixed at the inlet. The velocity profile at the inlet is also held constant, with the velocity magnitudes being derived from a power law formulation in the vicinity of the inner and outer no-slip surfaces.

2.5 TURBULENCE MODEL

A Baldwin-Lomax turbulence model (Ref. 6) was used to parameterize the turbulent shear stresses for the two-dimensional flow around a strut. In this approach, an eddy viscosity (μ_t) is calculated for an inner and an outer region. The eddy viscosity for the inner region is based on the Prandtl-Van Driest formulation

$$(\mu_t)_{inner} = \rho \ell^2 |\omega| \qquad (2)$$

where

$$\ell = ky\left[1.0 - \exp(-y^+/A^+)\right] \quad , \quad y^+ = \rho\sqrt{\tau_\omega}\,y/\mu \qquad (3)$$

and τ_ω is the wall shear stress. The magnitude of the vorticity $|\omega|$ is given by

$$|\omega| = \left[\left(\frac{\partial u}{\partial y} - \frac{\partial v}{\partial x}\right)^2 + \left(\frac{\partial v}{\partial z} - \frac{\partial w}{\partial y}\right)^2 + \left(\frac{\partial w}{\partial x} - \frac{\partial u}{\partial x}\right)^2\right]^{1/2} \qquad (4)$$

The eddy viscosity for the outer region is given by

$$\left(\mu_t\right)_{outer} = \rho\, KC_{cp}\, F_{wake}\, F_{kleb}\,(y) \qquad (5)$$

where F_{wake} is the smaller of $Y_{max}\, F_{max}$ or $C_{wk}\, Y_{max}\, U_d^2/F_{max}$.

11

F_{max} is the maximum value of the expression

$$F(y)=y|\omega| \left[1.0-\exp(-y^+/A^+)\right] \qquad (6)$$

in a profile and Y_{max} is y at that point. Also

$$F_{kleb}(y)= \left[1.0+5.5(yC_{kleb}/Y_{max})^6\right]^{-1} \qquad (7)$$

The quantity U_d is the difference between the maximum and minimum values of velocity in a given profile. The constants are assigned the following values: $A^+ = 26$, $C_{cp} = 1.6$, $C_{kleb} = 0.3$, $C_{wk} = 0.25$, and $K = 0.0168$.

As discussed by Mehta et al.(Ref. 7) the above formulation gives $\mu_t = 0.0$ in the wake region when the wake is symmetric, because the Van Driest damping function, Eq. (2), depends on the vorticity on the centerline of the wake, which has the value of zero. Mehta et al.correct for this error by modifying the length scale equation to give

$$\ell = 0.4y \left[1.0 - \exp \{-(y^+/A^+) - (x^+/A^+)\}\right] \qquad (8)$$

with

$$x^+ = \begin{cases} 0.0 \text{ if } x < x_b \\ (x - x_b)/L \text{ otherwise} \end{cases} \qquad (9)$$

x_b is the x location of the strut trailing edge, and L is the length of the strut.

In the outer region, the definition of F(y) is replaced by

$$F(y)=y|\omega| \left[1.0-\exp \{ -(y^+/A^+) - (x^+/A^+)\}\right] \qquad (10)$$

The eddy viscosity is determined at every point using Eqs. (2) and (5). The smaller of the two values is then used in the governing equations.

12

The turbulence model for the flow around a three-dimensional strut in an annulus is obtained by combining the Baldwin-Lomax model for flow around a two-dimensional strut described above with an approach similar to that of Chang et al. (Ref. 4) for flow in the HGM. In their analysis, which did not include the presence of struts, Chang et al adopted an extended Prandtl-Karman mixing length theory, with the mixing length (ℓ) given as

$$\frac{\ell}{\delta} = k^2 \left(1 - e^{-\tilde{z}/k}\right)\left(1 - e^{z^+/A^+}\right), \quad z^+ = \rho\sqrt{\tau_\omega}\, z/\mu \tag{11}$$

where $\tilde{z} = z/\delta$.

δ is some characteristic reference length scale which serves to divide the internal flow region into two zones. Figure 7 shows this approach applied to a two-dimensional channel flow. The terms δ_1 and δ_2 are the reference length scales measured from wall 1 and wall 2, respectively. In zone 1, δ_1 is used in Eq. (11), and $\tilde{z}$ and z^+ are computed based on wall 1. In zone 2, δ_2 is used in Equation 11, and $\tilde{z}$ and z^+ are computed based on wall 2. Various ideas have been proposed for δ, including the centerline of the flow domain, location of maximum velocity, and location of minimum vorticity (δ_ω), which is the length scale proposed by Chang et al. The calculations presented here also use δ_ω as the reference length scale.

The eddy viscosity in the three-dimensional strut in an annulus calculation is calculated first by computing μ_t according to Eqs. (2) through (10), which assumes that the strut is the only length scale. Next, μ_t is computed using Eq. (11), which assumes that the upper and lower annulus surfaces are the only scales, and ignores the presence of the strut. The smaller of the two values of μ_t is then taken as the final value of the eddy viscosity. This idea of calculating two separate eddy viscosities and then taking the smaller of the two values was applied by Gorski et al. (Ref. 8) to the problem of a wing on a single flat plate. It has been extended here to include the case of a strut between two walls.
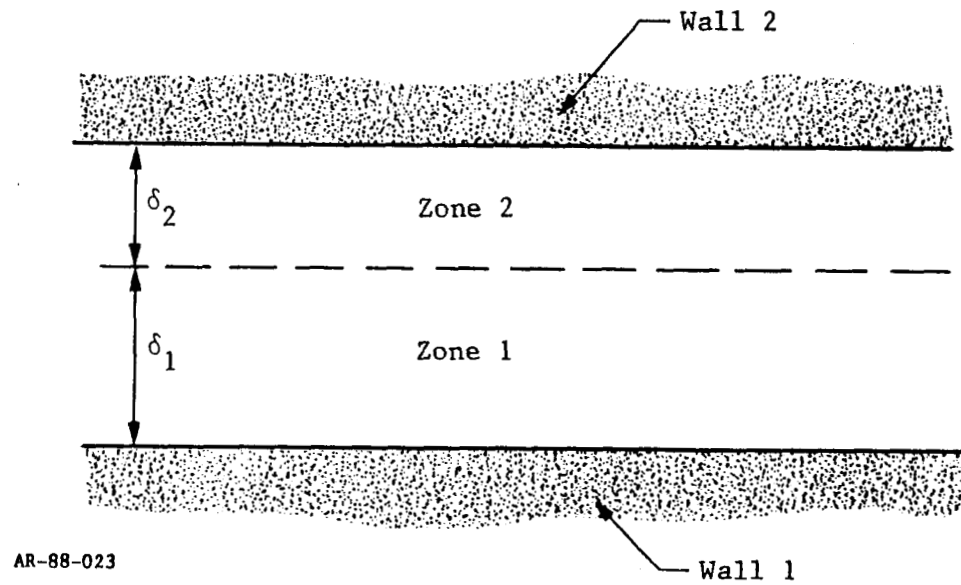
LOCKHEED-HUNTSVILLE ENGINEERING CENTER

Fig. 7 Mixing Length Regimes for Internal Flow

3. RESULTS

This section presents the laminar and turbulent numerical calculations
for two-dimensional flow around a strut, and three-dimensional flow around a
strut in an annulus. The results were produced using the graphical display
routine PLOT3D, which was developed at NASA-Ames Research Center (Ref. 9).

3.1 TWO-DIMENSIONAL COMPUTATIONS

Two-dimensional laminar and turbulent computations for flow around a strut
were performed. The Reynolds number (based on strut width) was 500 for the
laminar case and 1.9×10^6 for the turbulent case. The main purpose of these
calculations was to work out errors in the boundary and initial condition
routines, experiment with the Baldwin-Lomax turbulence model, and develop the
capability to perform multi-block calculations, which will be necessary in
simulating the flow in the complete three-dimensional HGM strut region.

3.1.1 Laminar

Figures 8 and 9 present velocity and pressure contours for a two-zone
laminar calculation of flow around two struts, with each zone representing one
strut. Two cases are considered, one without posts between the struts, and
one where the posts are included. The angle of incidence in both cases is
zero degrees.

As discussed previously, the posts are simulated by treating two lines
of nodes on the overlapping nodal planes as no-slip boundary nodes. Velocity
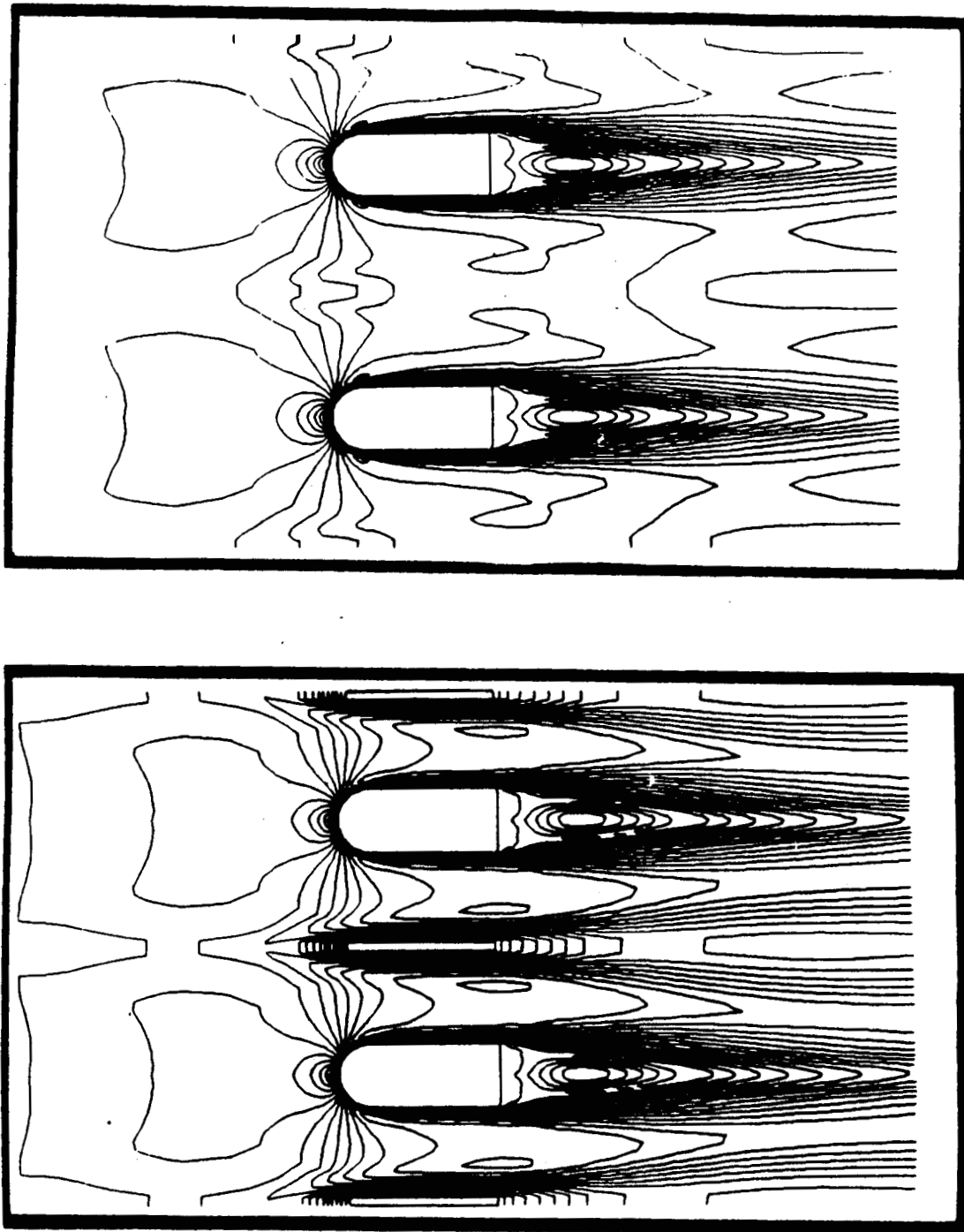vectors in the region of a post treated in this manner are presented in Fig.
10.

Fig. 8   Velocity Contours for Two Block Two-Dimensional Simulation
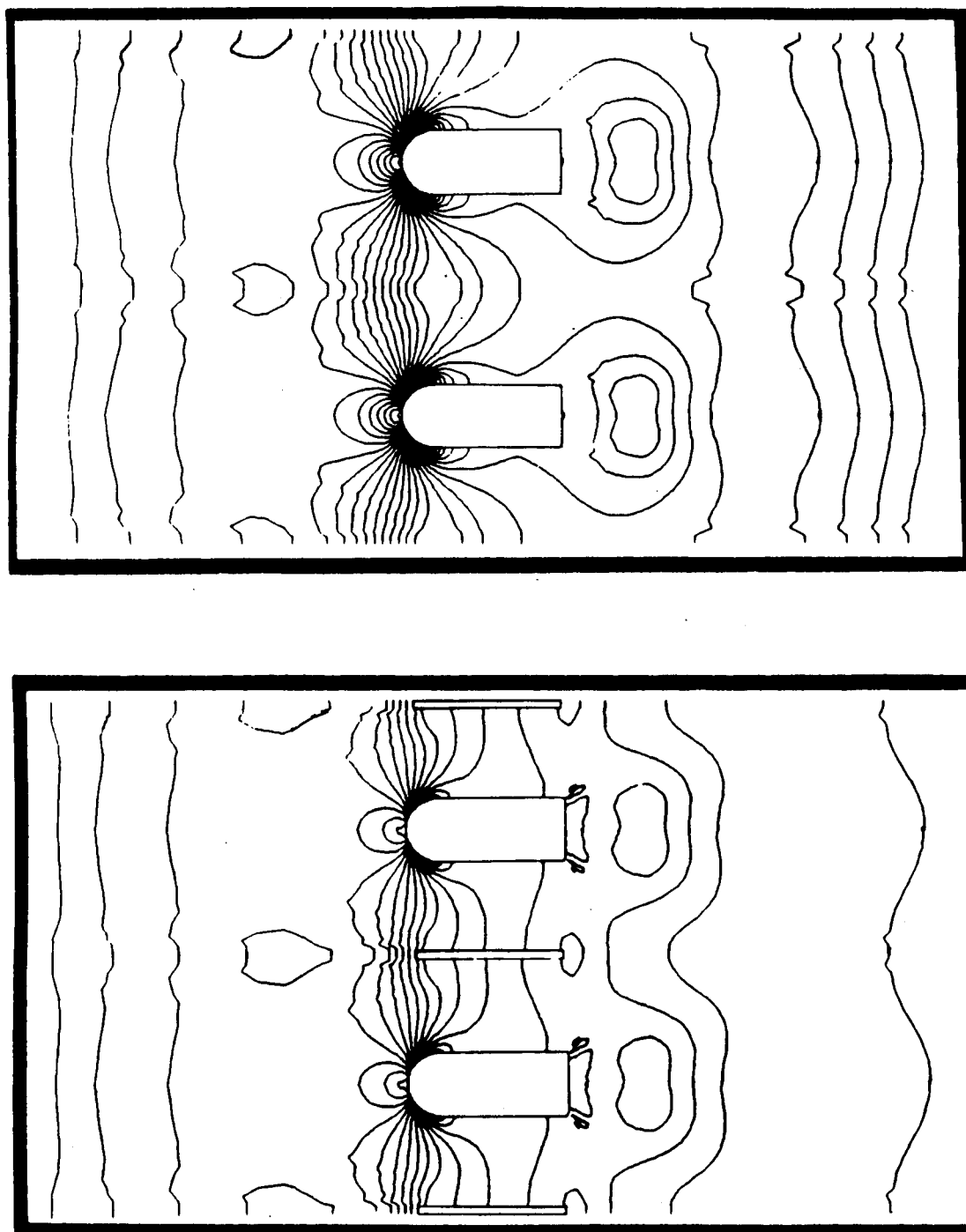of Two Struts with (Bottom) and Without Posts

LOCKHEED-HUNTSVILLE ENGINEERING CENTER

Fig. 9   Static Pressure Contours for Two Block Two-Dimensional Simulation
of Two Struts with (Bottom) and Without Spacers Included

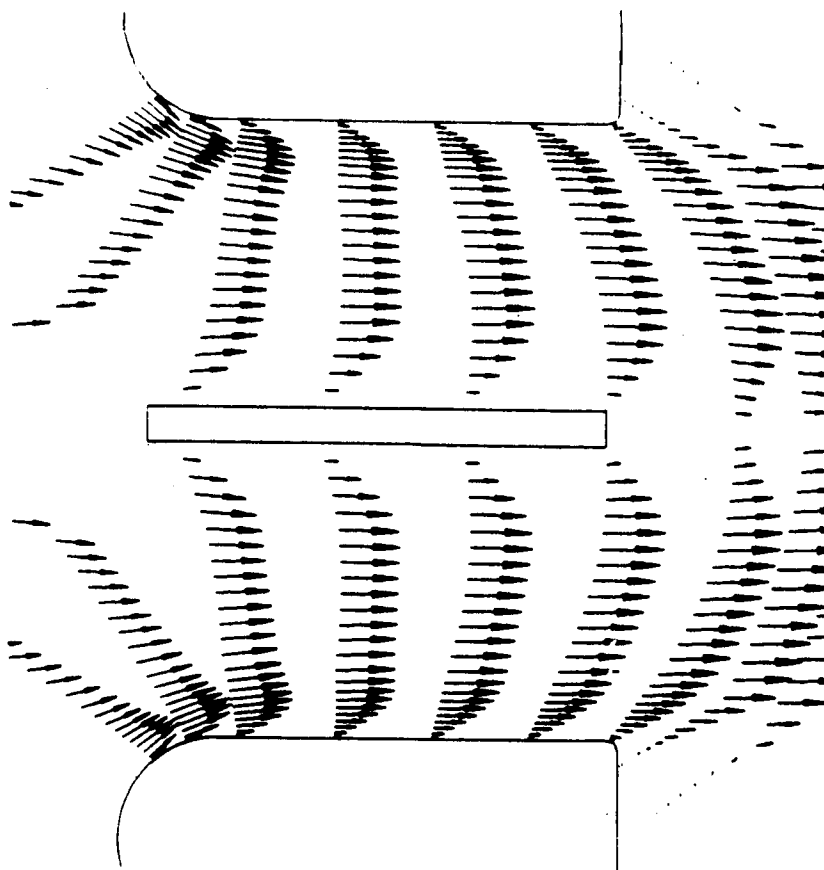LOCKHEED-HUNTSVILLE ENGINEERING CENTER

Fig. 10   Velocity Vectors Along Selected Nodal Lines in Region Between Two
Struts Showing Effect of Spacer Simulation Midway Between Them

Periodic boundary conditions are applied at the outer lateral boundaries of each zone to simulate the effect of a row of struts, or struts alternating with posts. The results in Figure 8 and 9 are seen to exhibit the expected periodic nature, with a period length of four strut widths.

Velocity vectors in the region immediately behind the strut, for the case without posts, are shown in Fig. 11. Two symmetric recirculation regions have developed, one on either side of the strut centerline. The length of the recirculation region is approximately two and a half strut widths.

The calculations discussed so far have been for zero angle of incidence. In addition to this, single block computations around a strut were performed with a 10-deg angle of attack. Results to date indicate that the flow is unsteady; this can be seen in Fig. 12, which shows the velocity contours at non-dimensional time step intervals of 1.0. Results at a Reynolds number of 50 did not display this unsteady appearance.

3.1.2 Turbulent

Single block turbulent computations (Re = 1.9 x 10^6) around a two-dimensional strut were performed at zero and 10-deg angle of incidence. A Baldwin-Lomax turbulence model was used to parameterize the turbulent shear stresses. Periodic boundary conditions were applied at the lateral boundaries. The grids used in the laminar computations discussed above were modified to obtain a finer resolution near the strut surface. The average value of y^+ at the first line of nodes above the strut was approximately ten. A more refined grid would undoubtedly have provided better resolution of the near-surface flow field. However, as mentioned previously, the main purpose of the two-dimensional computations was to experiment with the implementation of various aspects of the numerical procedure as a first step toward the complete three-dimensional flowfield simulation. As such, a value of $y^+ = 10$ is considered adequate for present purposes.
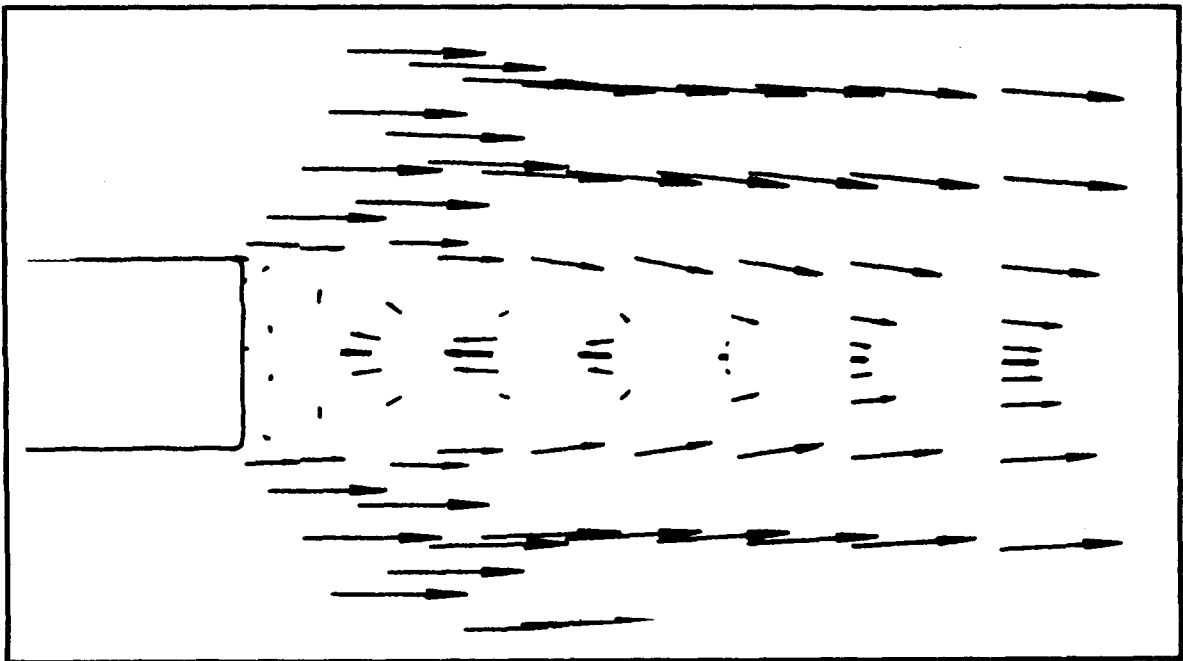
19

Fig. 11   Velocity Vectors Behind Strut for Two-Dimensional
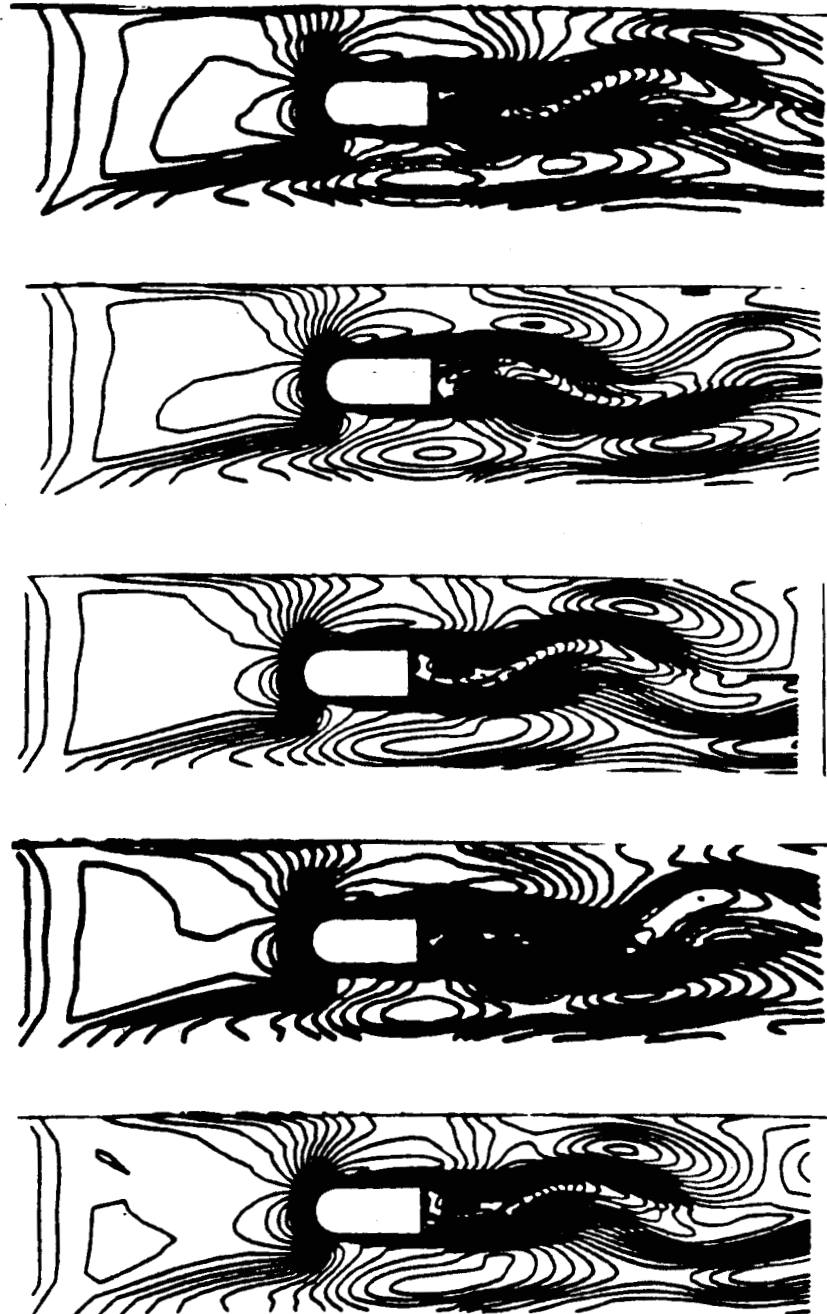Laminar Calculation Showing Recirculation Region

Fig. 12   Velocity Contours at Time Step of 1.0 for Two-Dimensional
Laminar Flow at 10-deg Angle of Attack

21

LOCKHEED-HUNTSVILLE ENGINEERING CENTER

Figure 13 shows the velocity contours around a strut for zero and 10-deg angle-of-attack. Velocity vectors in the near wake region for each of these cases is presented in Fig. 14. The size of the recirculation region is considerably smaller than for the laminar case (Fig. 11). As compared with the laminar 10-deg angle-of-attack results, the turbulent 10-deg angle-of-attack results did not show any noticeable unsteadiness in the velocity contours.

3.2 THREE-DIMENSIONAL COMPUTATIONS

Laminar (Re = 500) and turbulent three-dimensional (Re = 1.9×10^6) calculations were performed to simulate the three-dimensional flow around a strut in an annulus, as shown in Fig. 6. This kind of flow, which occurs when an obstruction is placed within an approaching boundary layer, is typically referred to as wing-body junction or corner flow. Perhaps its most dominant feature is a horseshoe vortex system that is caused by steep adverse pressure gradients set up at the junction of the obstruction (in this case the strut) and the body (i.e., the annulus). As a result of these pressure gradients, the vorticity in the oncoming boundary layer wraps around the obstruction in a characteristic horseshoe shape, with each leg having vorticity of opposite rotational sense.

Both the laminar and turbulent results displayed essentially the same flowfield features, including the presence of the characteristic horseshoe vortex system. Because of this, and because of their greater relevance to the HGM flow field, only the turbulent computations will be discussed here. The average value of y^+ on the first plane of grid points above the strut was approximately seven. On the lower and upper annulus surfaces the average value was about 1.5.

Figure 15 shows simulated oil flow lines on the lower and upper annulus surfaces, respectively. The oil flow lines are seen to diverge and wrap around the strut in the characteristic horseshoe shape. The size and shape of the horseshoe vortex system for the lower annulus surface is about the same as that of the upper surface.
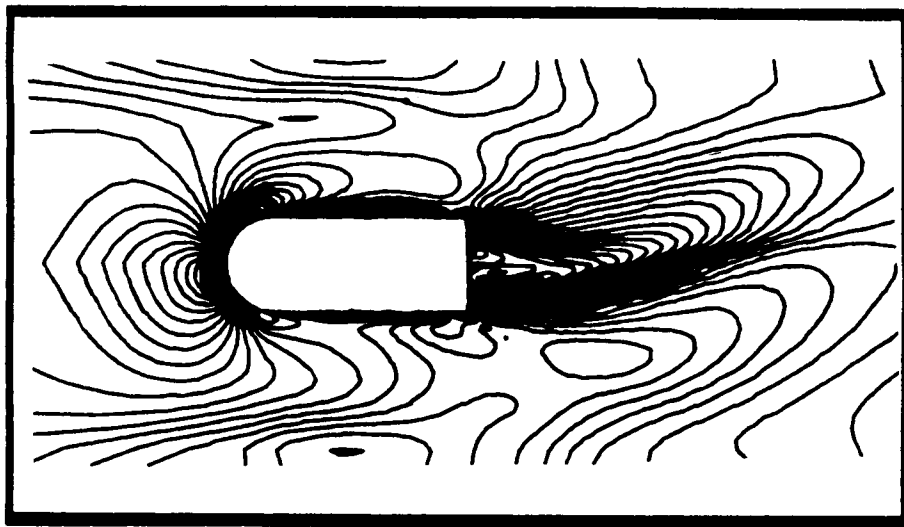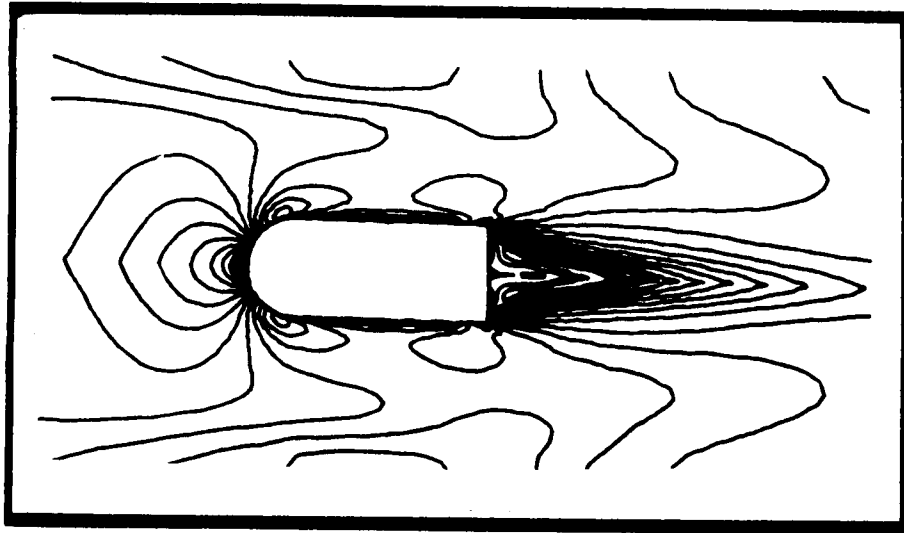
Fig. 13   Velocity Contours for Two-Dimensional Turbulent Flow at Zero (Top) and 10-deg Angle of Attack

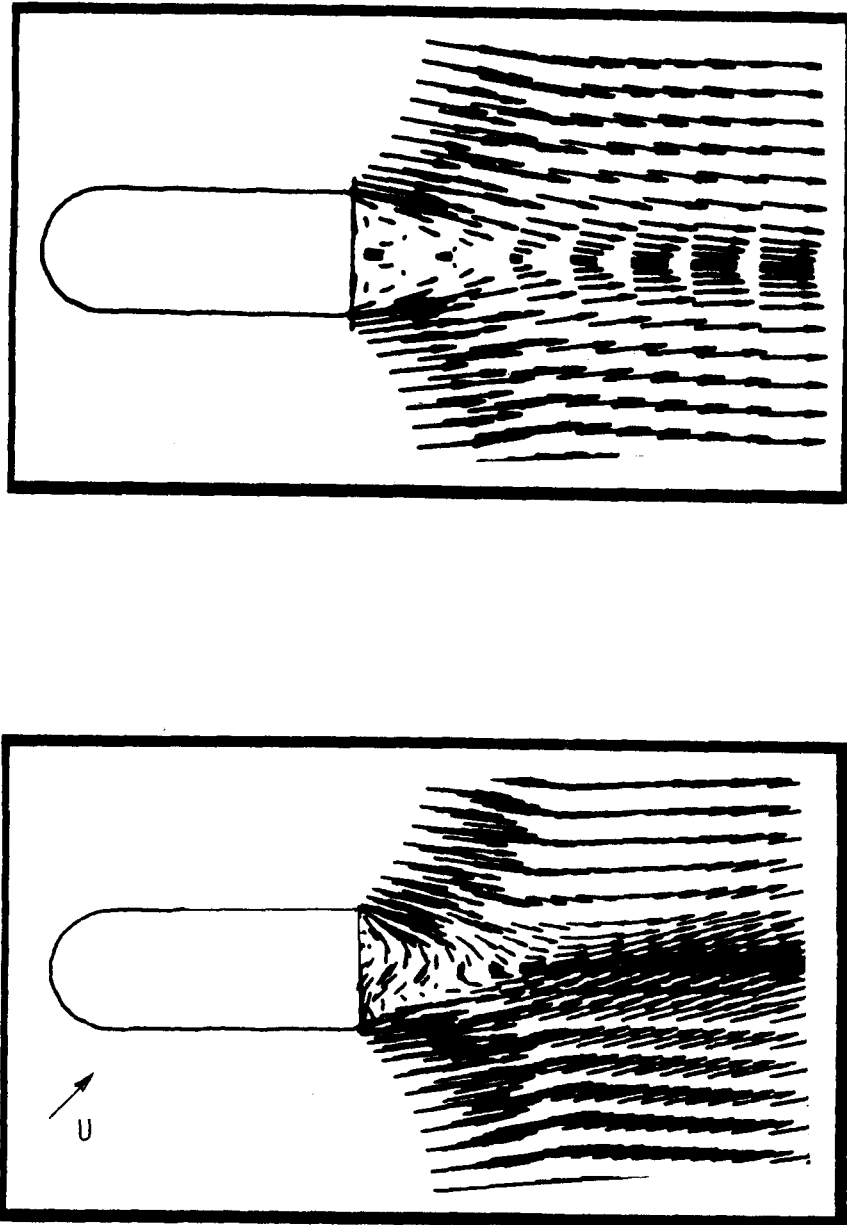LOCKHEED–HUNTSVILLE ENGINEERING CENTER

Fig. 14   Velocity Vectors Behind Strut for Two-Dimensional Turbulent
Flow at Zero (Top) and 10-deg Angle of Attack

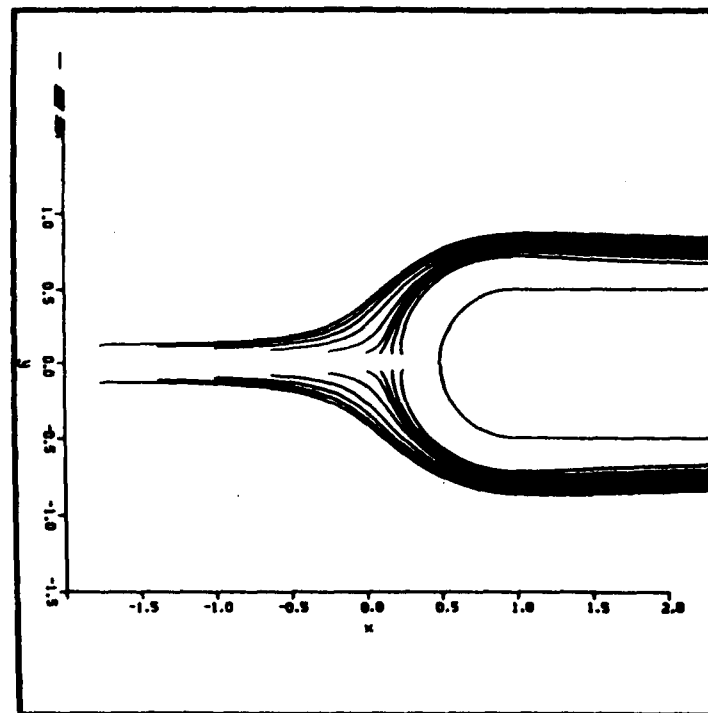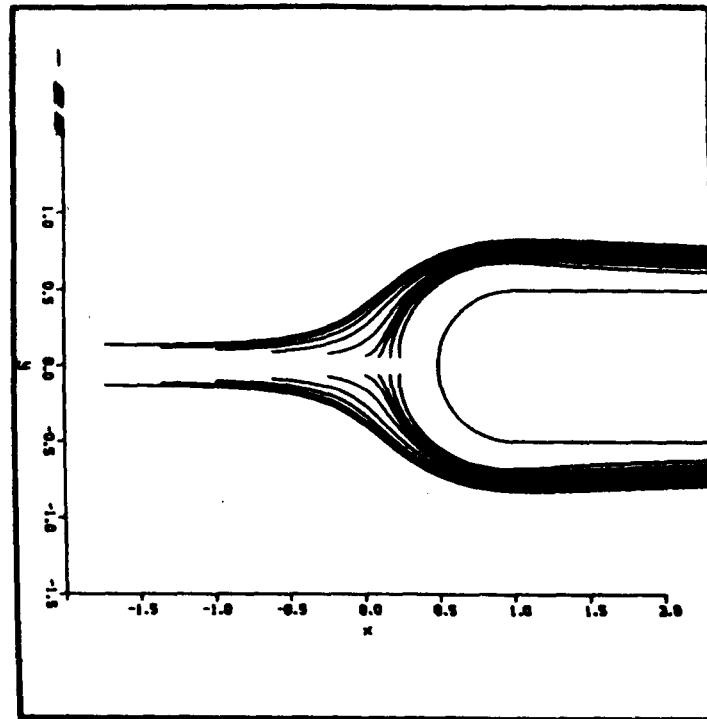Fig. 15   Simulated Oil Flow Streamlines at Upper (Top)
and Lower Annulus Surfaces

LOCKHEED–HUNTSVILLE ENGINEERING CENTER

Figure 16 presents particle traces for particles released at various points ahead of the strut. Two spiraling vortex systems are observed behind the strut; one system is associated with the lower annulus surface, and the second with the upper surface. The difference in size between the two systems is due to the asymmetry of the annulus geometry. A similar phenomenon has been found for laminar flow of a cylinder on a flat plate (Ref. 10).

Velocity vectors in the near-wake region of the strut midway between the annulus walls are presented in Fig. 17. The size of the recirculation region is approximately the same as for the turbulent flow around a two-dimensional strut, discussed earlier in Section 3.1.
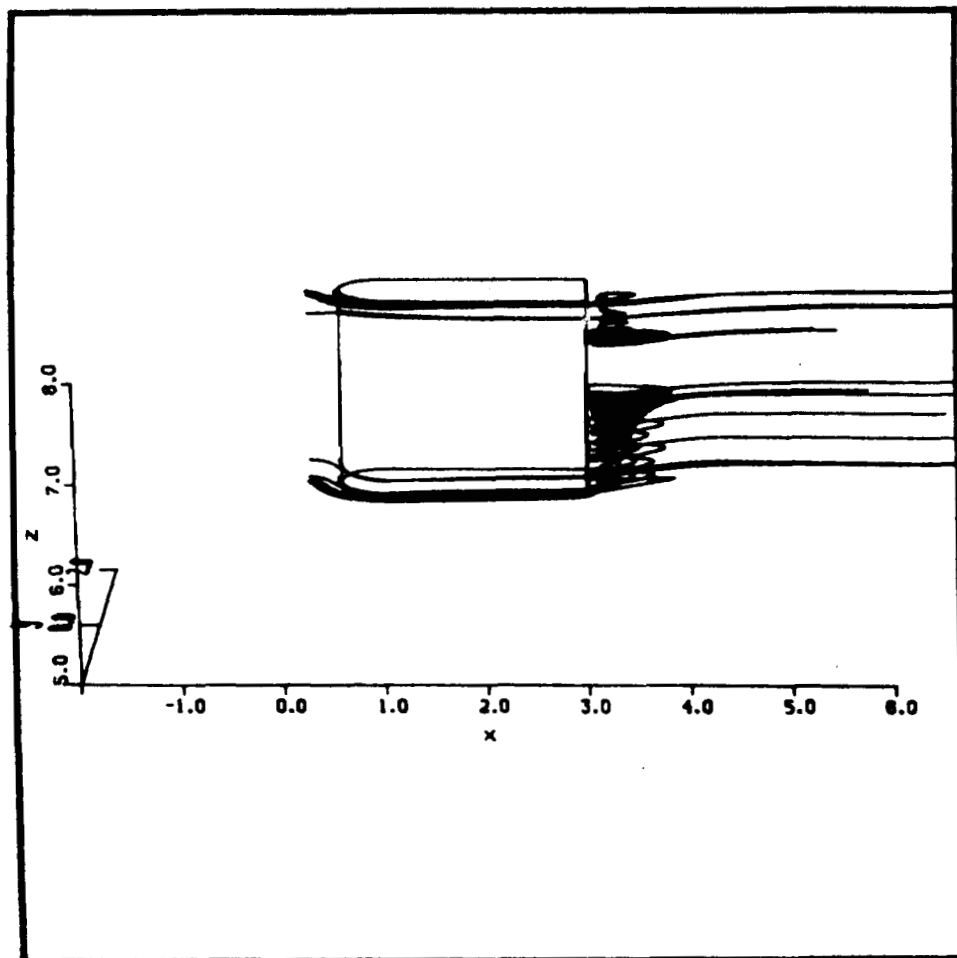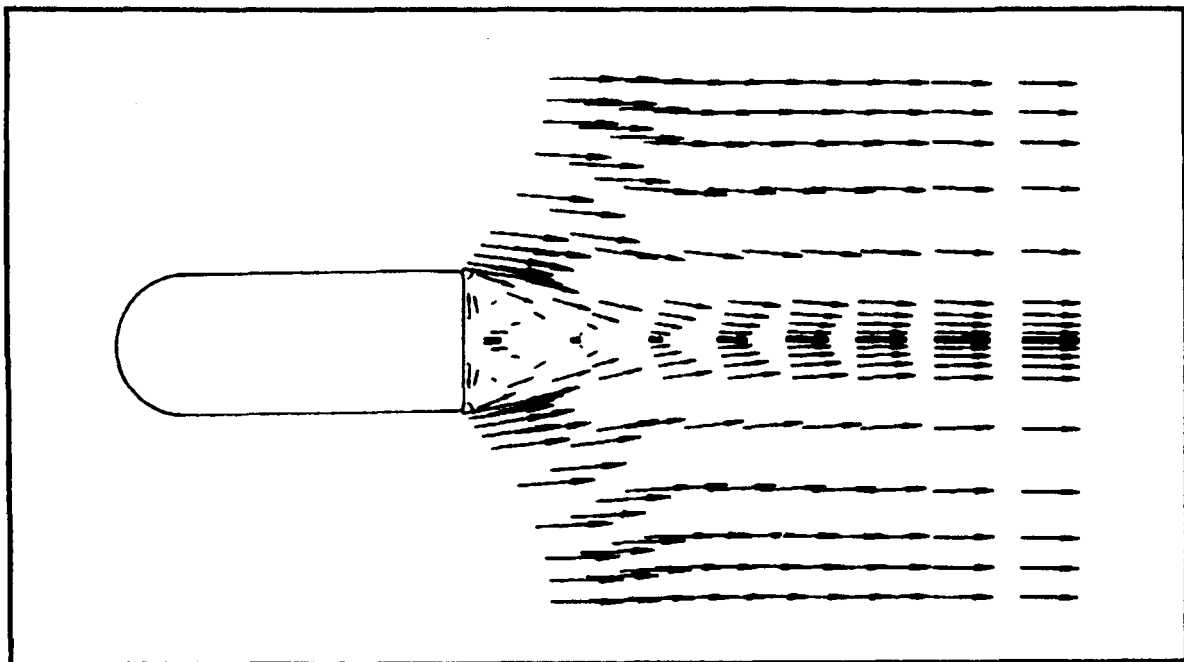
26

Fig. 16   Particle Traces

27

Fig. 17 Velocity Vectors Behind Strut Midway Between
Lower and Upper Annulus Surfaces

4. CONCLUDING REMARKS

This interim report has presented a numeral study, using the INS3D flow solver, of laminar and turbulent flow around two-dimensional strut, and three-dimensional flow around a strut in an annulus. A multi-block procedure was used to calculate two-dimensional laminar flow around two struts in parallel, with each strut represented by one computational block. Single block calculations were performed for turbulent flow around a two-dimensional strut, using a Baldwin-Lomax turbulence model to parameterize the turbulent shear stresses.

A modified Baldwin-Lomax model was applied to the case of a three-dimensional strut in an annulus. The results displayed the essential features of wing-body flows, including the presence of a horseshoe vortex system at the junction of the strut and the lower annulus surface. A similar system was observed at the upper annulus surface.

The test geometries discussed here were useful in developing the capability to perform multiblock calculations, and to simulate turbulent flow around obstructions located between curved walls. Both of these skills will be necessary to model the three-dimensional flow in the strut assembly of the SSME.

Work is now in progress on performing a three-dimensional two block turbulent calculation of the flow in the turnaround duct (TAD) and strut/fuel bowl juncture region. The grid for the TAD will comprise one computational zone and will be joined, using a two-plane overlap multiblock technique, to the strut/bowl grid, which will be a second computational zone. Only one strut will be considered with periodic boundary conditions to simulate a row of

struts. As a first step, the fuel bowl will be simulated by a streamwise variation of the cross-sectional area aft of the strut. This variation is shown in Fig. 18, which presents the revised strut grid. Later computations will incorporate a more detailed simulation of the fuel bowl, as well as the effect of the transfer ducts.
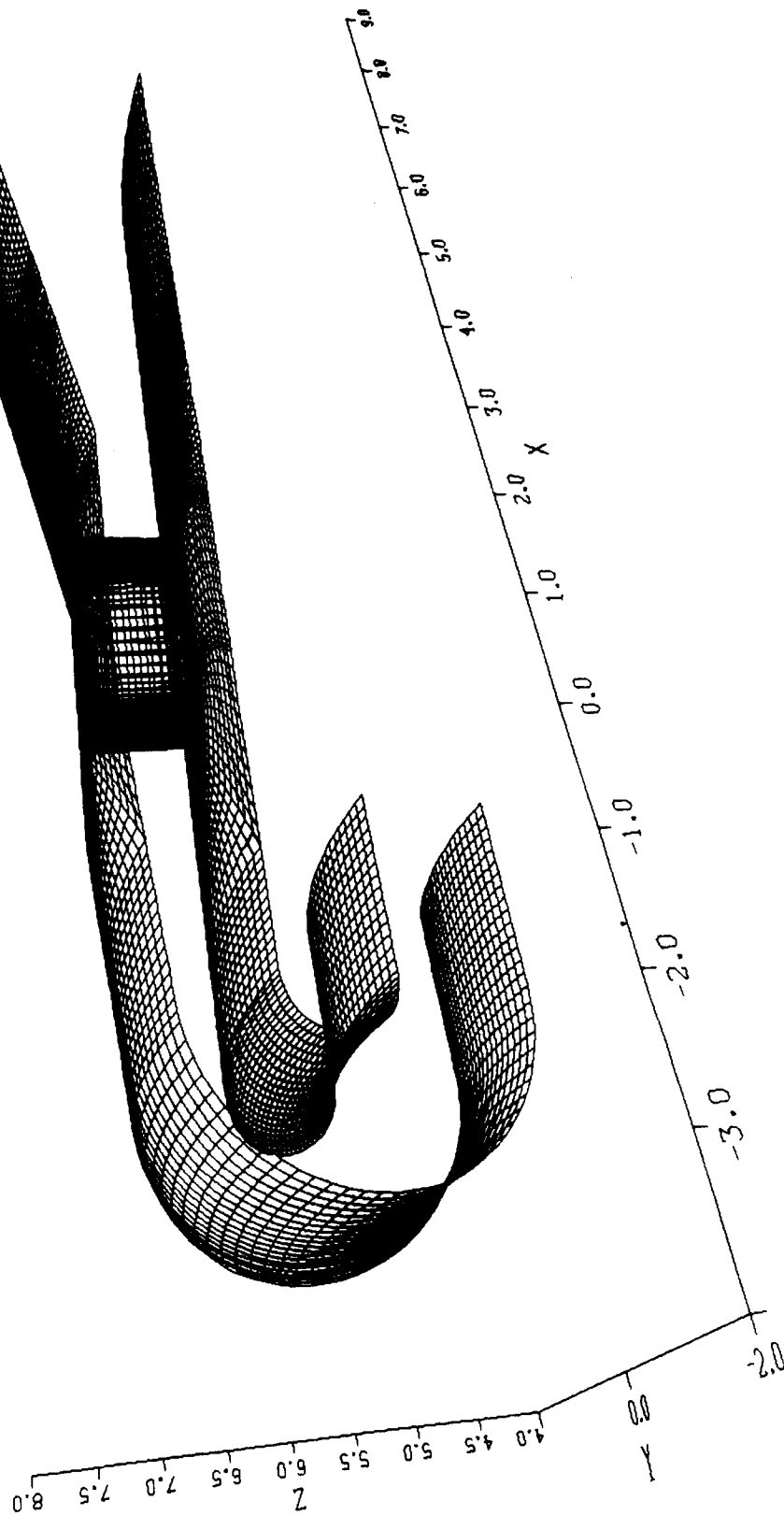
ORIGINAL PAGE IS
OF POOR QUALITY

Fig. 18 Computational Grid Showing Revised Geometry

31

5. REFERENCES

1. Kwak, D., J.L.C. Chang, S.P. Shanks, and S.R. Chakravarthy, "A Three-Dimensional Incompressible Navier-Stokes Flow Solver Using Primitive Variables," AIAA Journal, Vol. 24, 1986, pp. 390-396.

2. Hessenius, K.A., and M.M. Rai, "Applications of a Conservative Zonal Scheme to Transient and Geometrically Complex Problems," Computers and Fluids, Vol. 14, No. 1, 1986, pp. 43-58.

3. Walters, R.W., J.L. Thomas, and G.F. Switzer, "Aspects and Applications of Patched Grid Calculations," AIAA 86-1063, AIAA/ASME 4th Fluid Mechanics, Plasma Dynamics and Lasers Conference, Atlanta, Ga., 12-14 May 1986.

4. Chang, J.L.C., D. Kwak, S.C. Dao, and R. Rosen, "A Three-Dimensional Incompressible Flow Simulation Method and Its Application to the Space Shuttle Main Engine, Part I - Laminar Flow," AIAA-85-0175, AIAA 23rd Aerospace Sciences Meeting, Reno, 14-17 January 1985.

5. Holst, T.L., U. Kayivak, K.L. Gundy, S.D. Thomas, J.L. Flores, and N.M. Chanderjian, "Numerical Solution of Transonic Wing Flows Using an Euler/Navier-Stokes Zonal Approach," AIAA-85-1640, AIAA 23rd Aerospace Sciences Meeting, Reno, 14-17 January 1985.

6. Baldwin, B.S., and H. Lomax, "Thin Layer Approximation and Algebraic Model for Separated Turbulent Flows," AIAA Paper 78-257, Huntsville, Ala., January 1978.

7. Mehta, U., K.C. Chang, and T. Cebeci, "A Comparison on Interactive Boundary Layer and Thin-Layer Navier-Stokes Procedures," Numerical Physical Aspects of Aerodynamic Flows III, ed. T. Cebeci, Springer-Verlag, 1986.

8. Gorski, J.J., T.R. Govindran, and B. Lakshminarayana, "Computation of Three-Dimensional Turbulent Shear Flows in Corners," AIAA Journal, Vol. 23, No. 5, 1985, pp. 685-692.

9. Buning, P.G. and J.L. Steger, "Graphics and Flow Visualization in Computational Fluid Dynamics," Proceedings of the AIAA 7th Computational Fluid Dynamics Conference, Cincinnati, 1985.

10. Kaul, U.K., D. Kwak, and C. Wagner, "A Computational Study of Saddle Point Separation and Horseshoe Vortex Systems," AIAA-85-0182, AIAA 23rd Aerospace Sciences Meeting, Reno, 14-17 January 1985.